Kinetic model for activation-deactivation processes in solid catalysts

ARTICLE *in* INDUSTRIAL & ENGINEERING CHEMISTRY RESEARCH · JANUARY 1991

Impact Factor: 2.59 · DOI: 10.1021/ie00049a017

4 AUTHORS:

Ernesto Agorreta
Repsol
4 PUBLICATIONS **21** CITATIONS
SEE PROFILE

Jose-Angel Peña
University of Zaragoza
42 PUBLICATIONS **431** CITATIONS
SEE PROFILE

J. Santamaría
University of Zaragoza
285 PUBLICATIONS **5,011** CITATIONS
SEE PROFILE

Antonio Monzon
University of Zaragoza
104 PUBLICATIONS **1,914** CITATIONS
SEE PROFILE

A kinetic model for activation-deactivation processes in solid catalysts

Ernesto L. Agorreta, Jose A. Pena, Jesus Santamaria, and Antonio Monzon

Ind. Eng. Chem. Res., **1991**, 30 (1), 111-122 • DOI: 10.1021/ie00049a017

Eng. Chem. Process Des. Dev. 1981, 20, 262-273.
Tischer, R. E.; Narain, N. K.; Stiegel, G. J.; Cillo, D. L. Effect of Phosphorus on the Activity of Ni-Mo/Alumina Coal-Liquid Upgrading Catalysts. Ind. Eng. Chem. Res. 1987, 26, 422-426.
Vissers, J. P. R.; Bouwens, S. M. A. M.; de Beer, V. H. J.; Prins, R. The Promotion and Poisoning of the Hydrodesulfurization of Thiophene by Phosphate. Prepr.—Am. Chem. Soc., Div. Pet. Chem. 1986, 31, 227-230.

Received for review November 8, 1989
Revised manuscript received June 11, 1990
Accepted July 31, 1990

A Kinetic Model for Activation-Deactivation Processes in Solid Catalysts

Ernesto L. Agorreta, José A. Peña, Jesús Santamaria, and Antonio Monzón*

Department of Chemical Engineering, Faculty of Science, University of Zaragoza, 50009 Zaragoza, Spain

A kinetic model is proposed to describe the activation-deactivation phenomena taking place simultaneously with the main reaction on a catalytic surface. Potentially active sites are transformed into active sites by the activation process. Simultaneously, catalyst deactivation gives rise to deactivated sites from active sites. The model presented considers jointly the activation and deactivation processes on the catalyst surface. When activation processes are present, this is a more rigorous alternative to studies that only take into account catalyst deactivation. Kinetic expressions have been obtained for activation processes coupled with reversible and irreversible deactivation, and a study of the influence of the different kinetic parameters has been carried out. Finally, the model developed has been applied to previous literature data on *n*-butane isomerization on an aluminum chloride/sulfonic acid resin.

1. Introduction

Most kinetic studies dealing with catalyst deactivation usually consider a monotonic decrease of activity with time, until a constant value is reached, which can either be zero (complete deactivation) or different from zero (residual activity) (Fuentes, 1985; Corella et al., 1988). However, in many instances a different type of kinetic behavior has been reported, whereby the activity (or the reaction rate) versus time curves exhibit a maximum before starting the period of monotonic decrease. These types of curves have been found for a number of catalytic systems, including ethylene polymerization (McDaniel and Johnson, 1986), polymerization of benzyl alcohol (Olazar et al., 1988, 1989), alcohol dehydrogenation (Cunningham et al., 1986), hydrodesulfurization (HDS) processes (Brito et al., 1982; Laine et al., 1985), hydrodechlorination over a Pt catalyst (Noelke and Rase, 1979), and different reactions of CO and H_2, such as methanation (Amariglio et al., 1983; Hicks and Bell, 1984), CO oxidation (Perti and Kabel, 1985), methanol synthesis (Hicks et al., 1984), Fischer-Tropsch synthesis (Krebs et al., 1981; Dry, 1981; Pijolat et al., 1987; Tau and Bennet, 1985), and Kobel-Engelhardt synthesis (Kikuchi et al., 1984). A kinetic study of this type of system is interesting both because of the importance of the activation period for the operation of catalytic reactors (the activity at the maximum can be several times higher than the initial activity) and also because of the need for a more rigorous kinetic analysis of catalyst deactivation in systems where activation and deactivation processes are taking place simultaneously.

The model proposed in this work considers that the observed activity maxima arise from the joint effect of simultaneous activation and deactivation processes, as proposed by McDaniel and Johnson (1986), Amariglio and Amariglio (1981), and Kuivila et al. (1989). The increase in catalytic activity may be due to changes in the oxidation state of the active species in the catalyst, through the interaction of the catalytic surface with reactants and/or products (Montes et al., 1984; Cunningham et al., 1986; Nix et al., 1989), creation of surface defects by alternative oxidations and reductions during the catalyst pretreatment catalysts (Inioui et al., 1987), formation of new active species (Tau and Bennet, 1985; Bukur et al., 1989), an increase in the active area (Krebs et al., 1981), or atomic rearrangement of the active species on the surface (Amariglio et al., 1980, 1983; Kikuchi et al., 1984; Leary et al., 1986). Coke formation during the activation period has also been reported (Prada Silvy et al., 1988), which affects both the activation process and the residual activity.

Activation processes in the context of this work are different from (although obviously related to) the pretreatment processes required during the start-up stage in industrial catalytic reactors. On the other hand, catalyst deactivation could be due to any of the causes described in the literature. The model presented in this paper deals with both reversible and irreversible deactivation, as well as with different kinetic orders for the processes involved.

2. Model Development

The model presented in this paper considers three different states regarding the activity of the catalyst surface:

(i) Potentially Active. This corresponds to the potentially active sites (PAS) denoted by l* in the subsequent developments. These sites are capable of reaching the active state through physicochemical activation processes.

(ii) Active. This involves those sites that are active for the main reaction. Active sites (AS) are denoted by l.

(iii) Deactivated. This is the stage reached by the active sites that undergo deactivation processes, such as poisoning, coking, metal deposition, sintering, etc. Deactivated sites (DS) are denoted by l'.

0888-5885/91/2630-0111$02.50/0

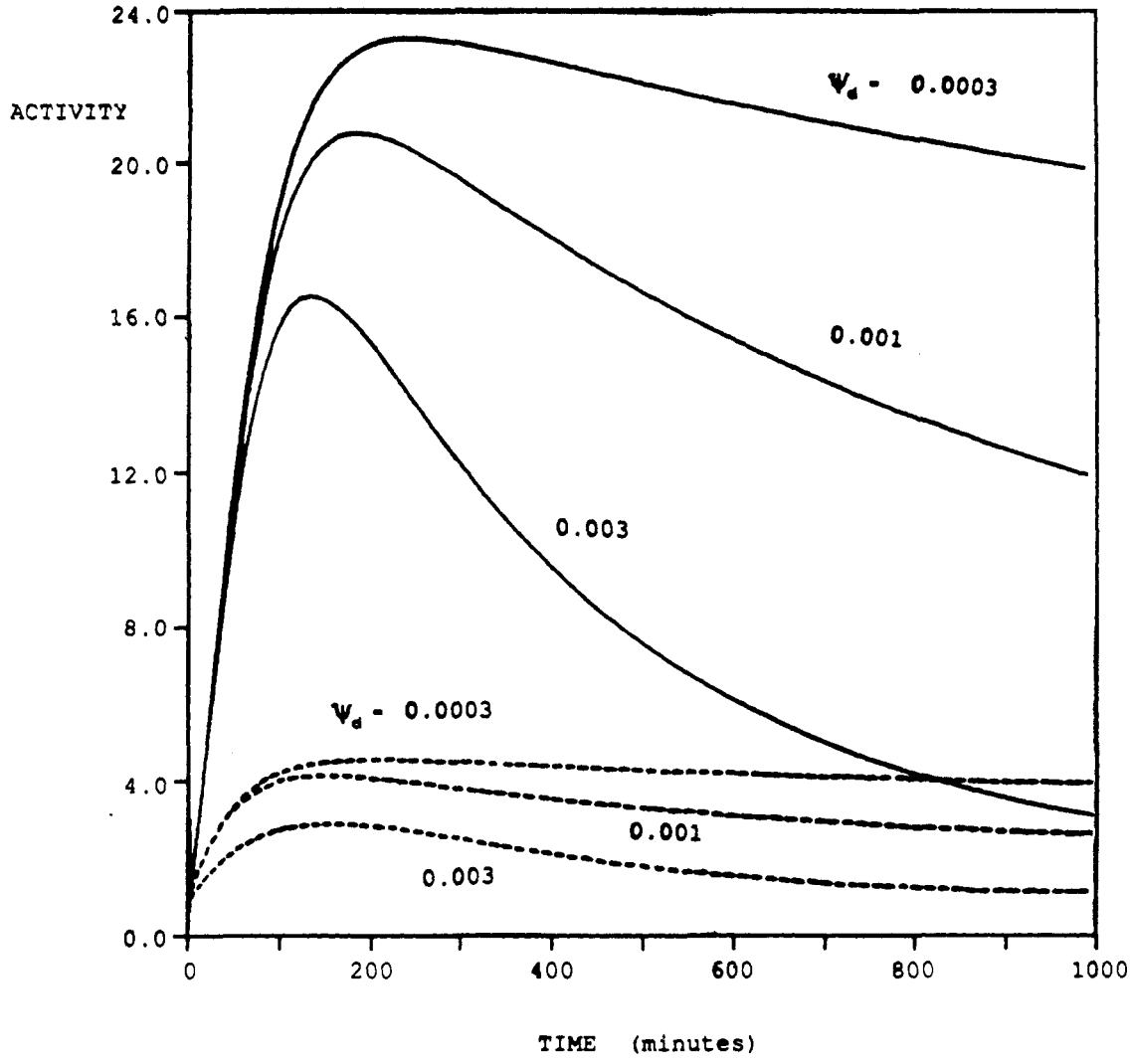

Figure 1. Activity versus time curves at $S = 0.8$ for different values of ψ_d and m ($m = 1$, discontinuous lines; $m = 2$, full lines).

Thus, we consider three processes taking place simultaneously on the catalyst surface:

main reaction $\quad A \rightleftharpoons R + S$

activation $\quad l^* \rightarrow l$

deactivation $\quad l \rightleftharpoons l'$

These processes occur according to the following kinetics:

(i) A LHHW expression has been assumed for the main reaction

$$-r_A = \frac{kL^m(p_A - p_R p_S/K)}{(1 + \sum K_i p_i)^m} a \qquad (1)$$

(ii) The activation process has been assumed to take place through the following mechanism:

(a) adsorption

$$M + l^* \rightleftharpoons Ml^*; \qquad K_M^* = C_{Ml}^*/(p_M C_l^*) \qquad (2)$$

(b) activation

$$eMl^* \rightarrow el + M'; \qquad -dC_l^*/dt = k_a p_M^e (C_l^*)^e (K_M^*)^e \qquad (3)$$

where M can be any reactant or product and M′ is a species resulting from the activation process.

(iii) Catalyst deactivation can be either reversible or irreversible. Thus, for instance, the following mechanism has been suggested for coke formation (Corella and Asúa, 1982):

(i) adsorption

$$N + l \rightleftharpoons Nl; \qquad K_N = C_{Nl}/p_N C_l \qquad (4)$$

(ii) deactivation

$$hNl + nN \rightleftharpoons Pl_h\downarrow + N' \qquad (5)$$

where the second process can be reversible, as indicated in eq 5. If the surface reaction is the controlling step in the process described, for the case of *irreversible* coking, the coke formation rate is given by

$$-dC_{Pl_h}/dt = k_d K_N^h p_N^{n+h} C_l^h \qquad (6)$$

whereas when coke deposition is *reversible* the corresponding expression is

$$-dC_{Pl_h}/dt = k_d K_N^h p_N^{n+h} C_l^h - k_d' p_{N'} C_{Pl_h} \qquad (7)$$

The three types of sites mentioned above (PAS, AS, and DS) must be taken into account when carrying out balances of sites on the catalyst surface, both initially and during the course of reaction. Thus, if L^* and L represent

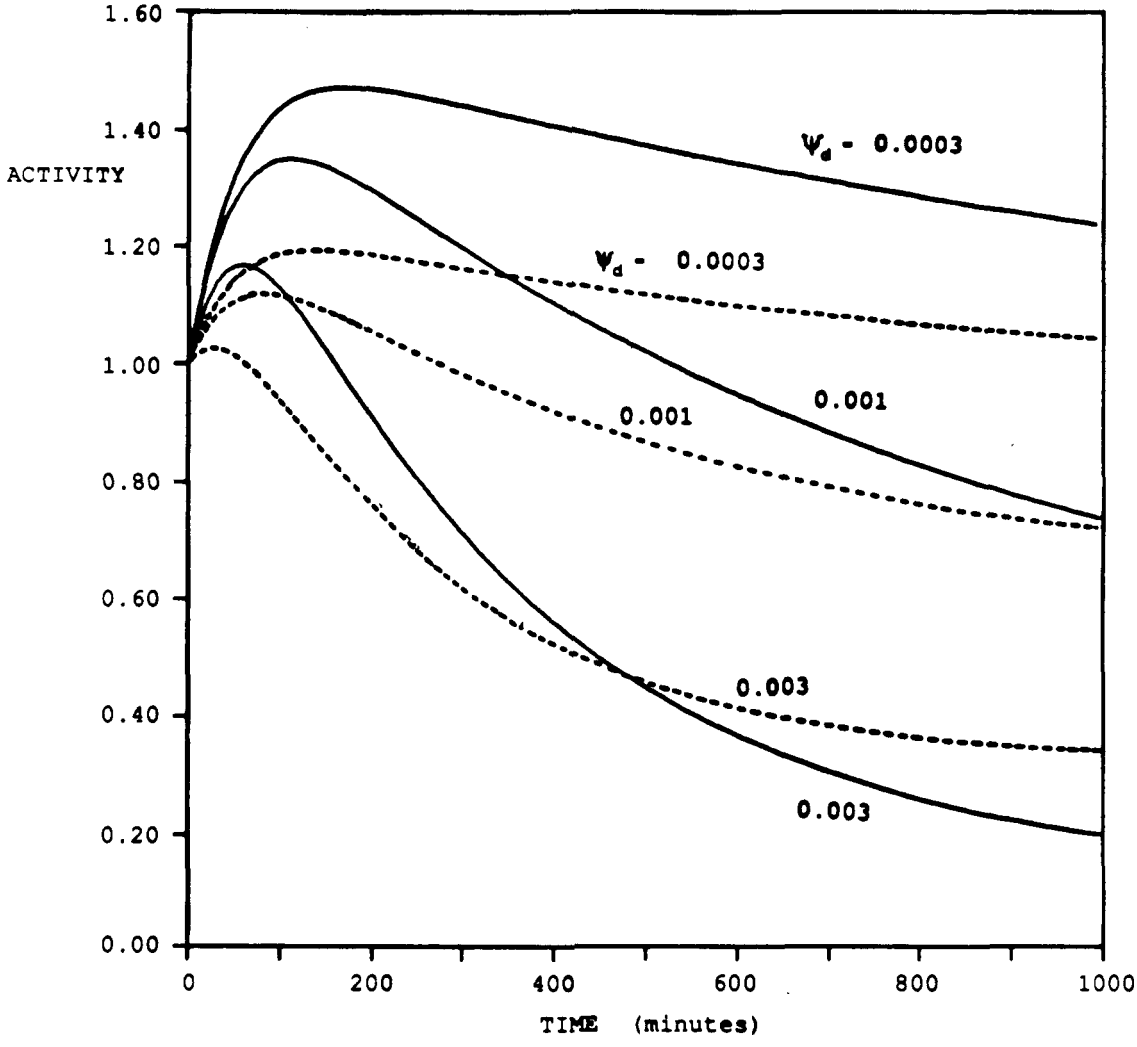

Figure 2. Activity versus time curves at $S = 0.2$ for different values of ψ_d and m ($m = 1$, discontinuous lines; $m = 2$, full lines).

the initial concentration of PAS and AS at $t = 0$, it follows that, at any time,

$$L + L^* = C_l^* + C_{Ml}^* + C_l + C_{Al} + C_{Rl} + C_{Sl} + C_{Nl} + hC_{Pl_h} \quad (8)$$

which shows that after a certain time on stream the initial sites can be vacant (C_l^*, C_l), covered by adsorbed species (C_{il}^*, C_{il}), or deactivated ($C_{l'} \equiv C_{Pl_h}$).

Taking into account the adsorption constants for each type of site (l^*, l), we can write

$$L + L^* = \alpha C_l^* + \beta C_l + hC_{l'} \quad (9a)$$

where

$$\alpha = 1 + K_M^* p_M \qquad \beta = 1 + \sum K_i p_i \quad (9b)$$

$$(i = A, R, S, N)$$

After differentiation of eq 9 with respect to time (assuming that α and β are approximately constant with time), the following expression is obtained

$$\alpha \frac{dC_l^*}{dt} + \beta \frac{dC_l}{dt} + h \frac{dC_{l'}}{dt} = 0 \quad (10)$$

Definition of Catalytic Activity. The solution of eqs 3, 10, and 6 or 7 yields the evolution of the concentrations of the different sites on the catalyst surface. However, it is customary to normalize these variables (C_l^*, C_l, $C_{l'}$) by defining the corresponding activities. Thus, a *potential activity* can be defined as the fraction of PAS that remains to be activated at a given time, i.e.,

$$a_p = \frac{\alpha C_l^*}{L^*} \quad (11)$$

On the other hand, according to the usual definition of *activity* (Szépe and Levenspiel, 1971; Corella and Asúa, 1982),

$$a = \frac{(-r_A)_t}{(-r_A)_0}\bigg|_{p_i;T} = \left(\frac{\beta C_l}{L}\right)^m \quad (12)$$

These definitions together with eq 5–7, 9, and 10 yield the evolution of the activity and of the potential activity:

(i) for reversible deactivation

$$-\frac{da}{dt} = -\frac{1}{1-S}\psi_s a^{d_m} + \psi_s a - \frac{S}{1-S} m\psi_s a^{d_m} a_p^e + \frac{S}{1-S}\psi_s a^{d_m} a_p + \psi_d a^d \quad (13)$$

(ii) for irreversible deactivation

$$-\frac{da}{dt} = -\frac{S}{1-S} m\psi_s a^{d_m} a_p^e + \psi_d a^d \quad (14)$$

In addition, the evolution of the potential activity is given by

$$-\frac{da_p}{dt} = \psi_a a_p^e \tag{15}$$

In these equations, the following parameters have been used:

$$S = \frac{L^*}{L + L^*}; \qquad d = \frac{m + h - 1}{m}$$

$$d_m = \frac{m - 1}{m}; \qquad \psi_s = m k_d' p_N^{\prime}$$

$$\psi_a = \frac{k_a (L^*)^{e-1} (K_M^*)^e p_M^e}{\alpha^{e-1}}$$

$$\psi_d = \frac{mhk_d L^{h-1} K_N^{n+h} p_N^{n+h}}{\beta^h} \tag{16}$$

Equations 13 and 15 correspond to a rather general kinetic model, which in fact includes other previously proposed models (Corella and Asúa, 1982; Corella et al., 1988; Agorreta et al., 1988). Also, eq 14 is obviously a particular case of eq 13 ($k_d' = 0$, and therefore $\psi_s = 0$, for irreversible deactivation). If activation processes were absent, $k_a = 0$, and therefore, $\psi_a = 0$. Under these conditions, eq 13 becomes

$$-da/dt = -\psi_s a^{d_m} + \psi_s a + \psi_d a^d \tag{17a}$$

and for the case in which $m = h = 1$, eq 17a becomes

$$-\frac{da}{dt} = (\psi_s + \psi_d)\left(a - \frac{\psi_s}{\psi_d + \psi_s}\right) = (\psi_s + \psi_d)(a - a_s) \tag{17b}$$

which has been used to represent reversible deactivation (Fuentes, 1985; Corella et al., 1988). Finally, for an irreversible deactivation in the absence of activation processes, we obtain

$$-da/dt = \psi_d a^d \tag{18}$$

widely employed in the kinetic modeling of relatively simple deactivation processes.

Equations 13 and 15 (reversible deactivation) can be solved analytically for the case $e = h = m = 1$. Under these conditions, for an isothermal differential reactor, we obtain

$$a = a_s + B \exp(-\psi_a t) + (1 - a_s + B) \exp\{-(\psi_d + \psi_s)t\} \tag{19}$$

$$a_p = \exp(-\psi_a t) \tag{20}$$

where

$$a_s = \frac{1}{1 - S} \frac{\psi_s}{\psi_d + \psi_s} \tag{21a}$$

$$B = \frac{S}{1 - S} \frac{\psi_a - \psi_s}{\psi_d + \psi_s - \psi_a} \tag{21b}$$

For irreversible deactivation ($\psi_s = 0$), the solution of eqs 14 and 15 for $e = m = h = 1$ yields

$$a = C \exp(-\psi_a t) + (1 - C) \exp(-\psi_d t) \tag{22}$$

where

$$C = \frac{S}{1 - S} \frac{\psi_a}{\psi_d - \psi_a} \tag{23}$$

The model described by eqs 13 and 15 predicts the appearance of a maximum in activity, a_{max} at a time t_{max}, as well as a residual activity a_s for time $t = \infty$ (a_s would be null for irreversible deactivation, $\psi_s = 0$). The calculation of a_{max}, t_{max}, and a_s generally involves the use of numerical methods. However, for $e = h = m = 1$, an analytical solution can be obtained:

(i) reversible deactivation

$$t_{max} = \frac{1}{\psi_a - \psi_d - \psi_s} \ln \frac{B\psi_a}{(a_s - B - 1)(\psi_d + \psi_s)} \tag{24}$$

(ii) irreversible deactivation

$$t_{max} = \frac{1}{\psi_a - \psi_d} \ln \frac{S\psi_a^2}{\psi_d[\psi_a - \psi_d(1 - S)]} \tag{25}$$

From this expression and from eq 21, it is clear that both a_{max} (which is found by substituting t_{max} instead of t in eq 19) and a_s depend on the initial state of the catalyst (S) and on the operating conditions (through ψ_a, ψ_d, and ψ_s).

3. Parametric Study of the Model

Given the fact that the model equations do require numerical solution in most cases and that there is a considerable number of parameters involved, a parametric study has been carried out in order to assess the effect of each of the main parameters on three measurable responses of the system, namely, the maximum activity obtained, a_{max}, the time at which this activity is reached, t_{max}, and the potential activity at time equal to t_{max}, a_{pm}, which is a measure of the fraction of initial PAS that remain as such (i.e., unconverted to AS), when the maximum activity a_{max} is reached. The following parameters have been analyzed: ψ_a, ψ_s, ψ_d, S, m, e, and h.

The activation, deactivation, and regeneration functions, ψ_a, ψ_d, and ψ_s, depend on temperature as well as on the composition of the reacting mixture. If LHHW kinetics are assumed, this would introduce a number of additional parameters. Therefore, in this study, ψ_a, ψ_s, and ψ_d are taken as constants. This implies certain physical restrictions such as isothermicity, homogeneous and constant reaction environment, etc. The study of the model for conditions under which these assumptions do not hold will be presented in a separate paper (Agorreta et al., 1990).

Some of the parameters varied in the study cannot usually be altered in practice by means of changes in the operating conditions or in catalyst pretreatment. Such is the case of the kinetic orders e, m, and h. Thus, studying the effect of the kinetic orders is in fact equivalent to studying different reaction systems. On the other hand, the rest of the parameters listed above depend on operating and/or pretreating conditions and can be manipulated experimentally in order to optimize a given reaction system.

The method used for the parametric study is a modification of the procedure described by Box et al. (1978) for multiple-level factorial design. The relevant definitions and the description of the method used in our case are given in the Appendix at the end of this paper.

Interaction Effects. The initial fraction of PAS, S, defined in eq 16, determines to a large extent the effect that a variation in the values of one of the remaining parameters has on the three system responses studied.

This is illustrated in Figures 1 and 2, where it can be observed that the change that a_{max} undergoes when m is increased from 1 to 2 strongly depends on the value of the

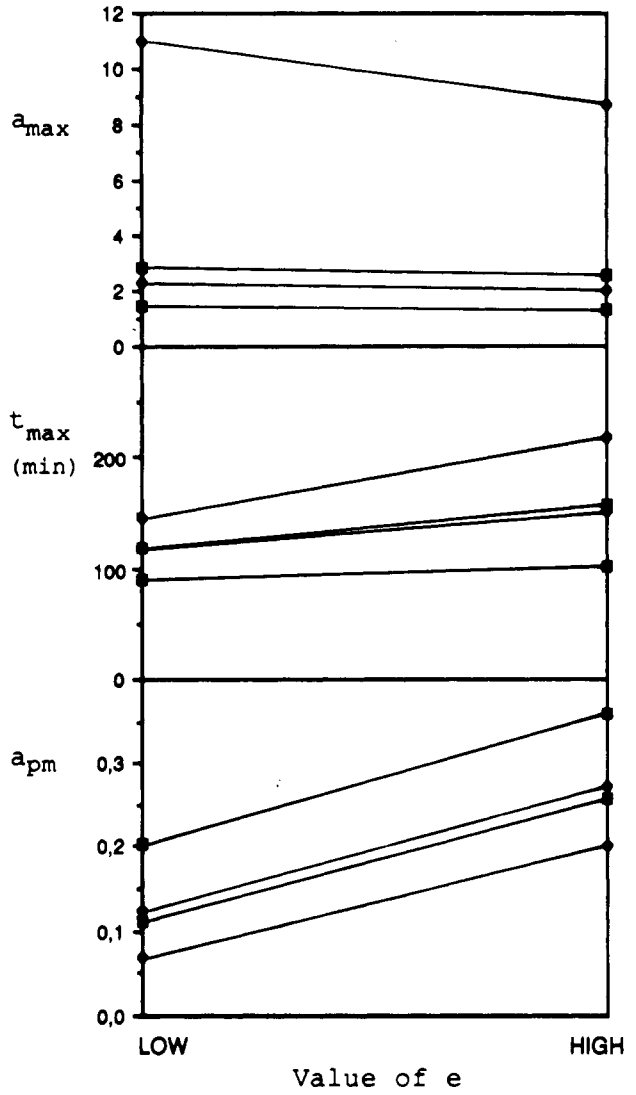

Figure 3. Effect of the variation of the kinetic order for the activation reaction, e. A, top; B, middle; C, bottom. (□) m = 1, low S; (◆) m = 2, low S; (■) m = 1, high S; (◇) m = 2, high S.

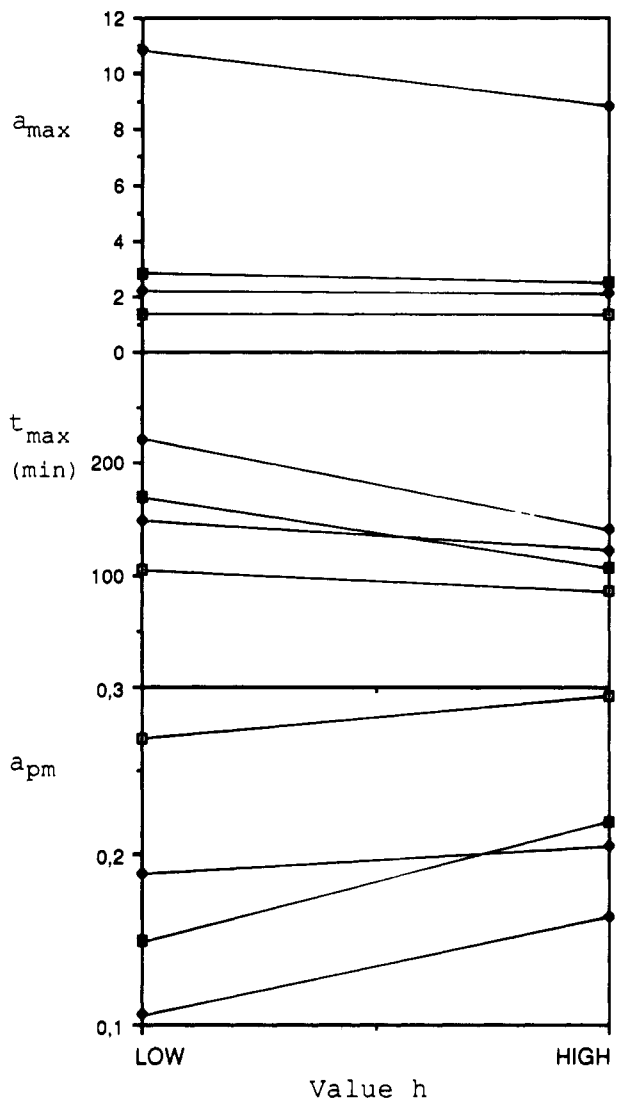

Figure 4. Effect of the variation of the kinetic order for the deactivation reaction, h. A, top; B, middle; C, bottom. (□) m = 1, low S; (◆) m = 2, low S; (■) m = 1, high S; (◇) m = 2, high S.

Table I. Parameter Interactions in Reference to a_{max}

m	e	h	ψ_a	ψ_d	S (high/low)
m	-1.363	-1.094	2.101	-1.075	0.594/5.784
e		0.0245	0.002	-0.008	-0.134/-1.022
h			0.142	-0.1013	-0.059/1.624
ψ_a				0.485	-0.218/-1.624
ψ_d					-0.234/-1.663

Table II. Average Values of a_{max}, t_{max}, and a_{pm} for Different Combinations of Values of m and S

values of m and S	a_{max}	t_{max}, min	a_{pm}
m = 1, low S	1.373	95.02	0.282
m = 2, low S	2.163	135.4	0.198
m = 1, high S	2.668	181.9	0.184
m = 2, high S	9.856	181.9	0.135

initial fraction of PAS: For high values of S (low initial activity, most sites as PAS), an increase in m from 1 to 2 increases over 5 times the ratio of the maximum activity obtained to the initial activity, Figure 1, whereas the effect shown in Figure 2 (low values of S) is considerably weaker.

Thus, there is an interaction between m and S; i.e., the magnitude of the effect produced by a change in m depends on the value of S. This interaction, termed mS, has a value of 2.252 (see the Appendix for calculations), which means that the effect of the variation of m from 1 to 2 on a_{max} is, on average, 2.252 units higher for S = 0.2 than for S = 0.8. Taking into account the results shown in the Appendix (the average value for a_{max} in the 144 simulations carried out is 4.02 units, and the main effect of m on a_{max} is -3.979), the value of mS obtained indicates a strong interaction between both parameters, which is consistent with the behavior shown in Figures 1 and 2.

The interactions among the other parameters studied in this work are summarized in Table I, where two columns have been used for S, corresponding to the low (i.e., from 0.2 to 0.5) and high (from 0.5 to 0.8) ranges of variation of S.

The results in Table I show a strong interaction of m with all other parameters. For this reason, the cases of different kinetic orders for the main reaction are studied separately in this work. In the same way, for high values of S, a strong interaction with other parameters appears, which led us to a further division in the study: high initial activity (S < 0.5) and low initial activity (S > 0.5). The average values of the three system responses studied are shown in Table II for the four cases mentioned above. These can serve as a reference to study the main effects of the different parameters, which are discussed next.

Influence of the Kinetic Orders m, e, and h. In

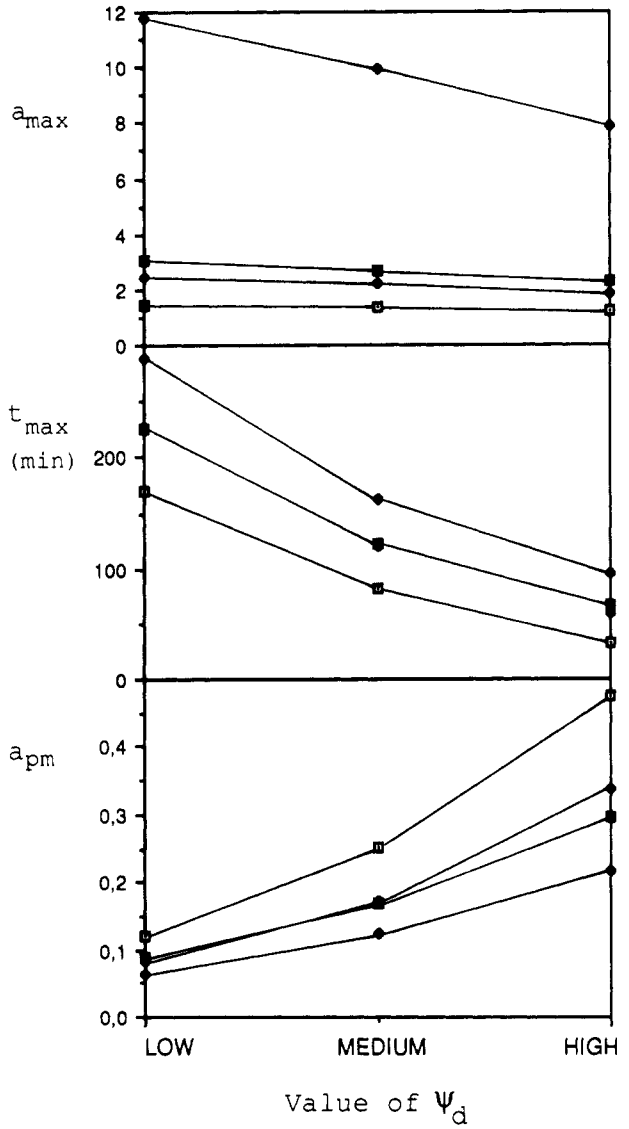

Figure 5. Effect of the variation of the activation function, ψ_a. A, top; B, middle; C, bottom. (□) m = 1, low S; (◆) m = 2, low S; (■) m = 1, high S; (◇) m = 2, high S.

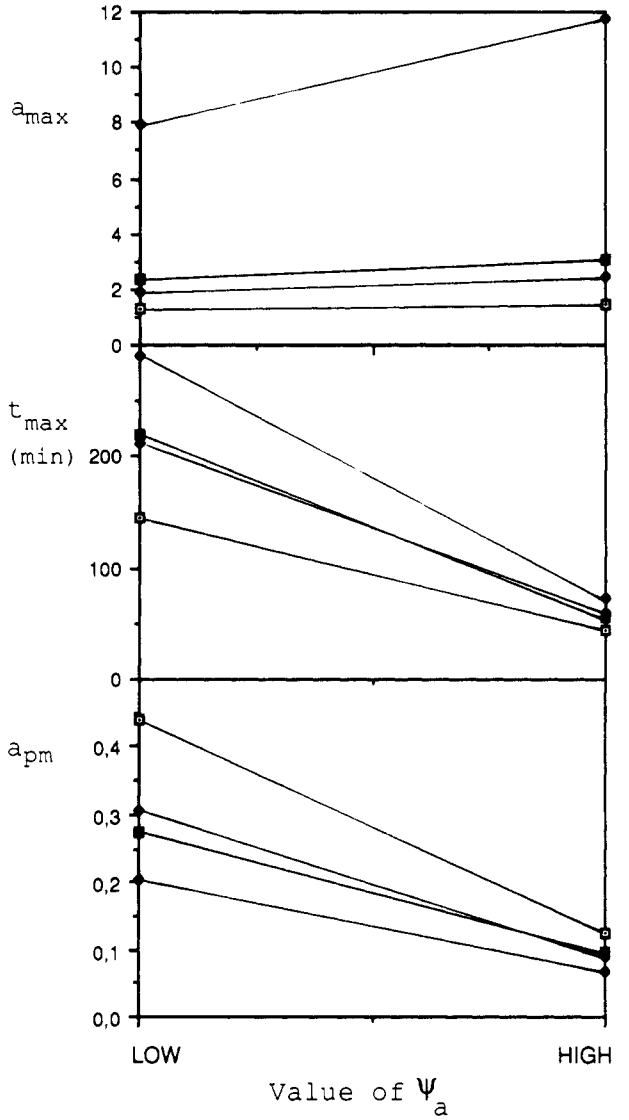

Figure 6. Effect of the variation of the deactivation function, ψ_d. A, top; B, middle; C, bottom. (□) m = 1, low S; (◆) m = 2, low S; (■) m = 1, high S; (◇) m = 2, high S.

spite of the strong interaction of the kinetic order of the main reaction, m, the general trends are clear from the results in Table II: A higher value of m means an increase in the maximum activity obtained, a lower value of a_{pm} and a delayed appearance of the activity maximum.

The effect of the kinetic order of the activation reaction is less marked than that of m. Thus, Figure 3A shows that the effect of e on a_{max} is only relevant at high values of S (low initial activity) and m. In this case, increases in e give rise to a decrease in the maximum activity obtained, whereas in all the other cases studied changes in e show little influence. On the other hand, Figure 3B shows that increasing e will increase t_{max}, whatever the values of m and S, although again the effect is more pronounced for higher values of these. The increase in t_{max} is a consequence of the slower activation process, which takes place for higher values of e. The same circumstance is the cause of the behavior shown in Figure 3C: An increase in e gives rise to a higher fraction of PAS at t_{max}.

A similar situation is obtained for the kinetic order of the deactivation reaction, h (Figure 4): An increase in the value of h causes a significant decrease in a_{max} for high values of m and S, whereas the effect seems negligible for all other cases. In addition, lower values of t_{max} and higher values of a_{pm} are obtained when h is increased. These two responses are related; i.e., since the evolution of a_p only depends on ψ_a and e (eq 15), the influence of other parameters on a_{pm} takes place exclusively through alterations of the value of t_{max}. A lower value of t_{max} means a higher value of a_{pm}, since there is less time available for the decrease of potential activity.

Influence of the Activation and Deactivation Functions. The effect of the activation function ψ_a on a_{max} is shown in Figure 5A. It can be observed that the general trend is toward an increase in the maximum activity obtained when increasing ψ_a, especially at high values of m and S. The values of t_{max} correspondingly decrease (Figure 5B), which was an expected result since a higher value of ψ_a implies a faster conversion of PAS into AS. It is also interesting to note that the curves for low m and high S and for high m and low S are almost coincident, which seems to indicate that their effects on t_{max} balance each other in this case. The behavior of a_{pm} (Figure 5C) is consistent with the above case; i.e., a_{pm} decreases for faster activation processes (higher values of ψ_a).

The results of the study of the effect of the deactivation function ψ_d (which was carried out at three levels) are shown in Figure 6. It can be seen that the values of the

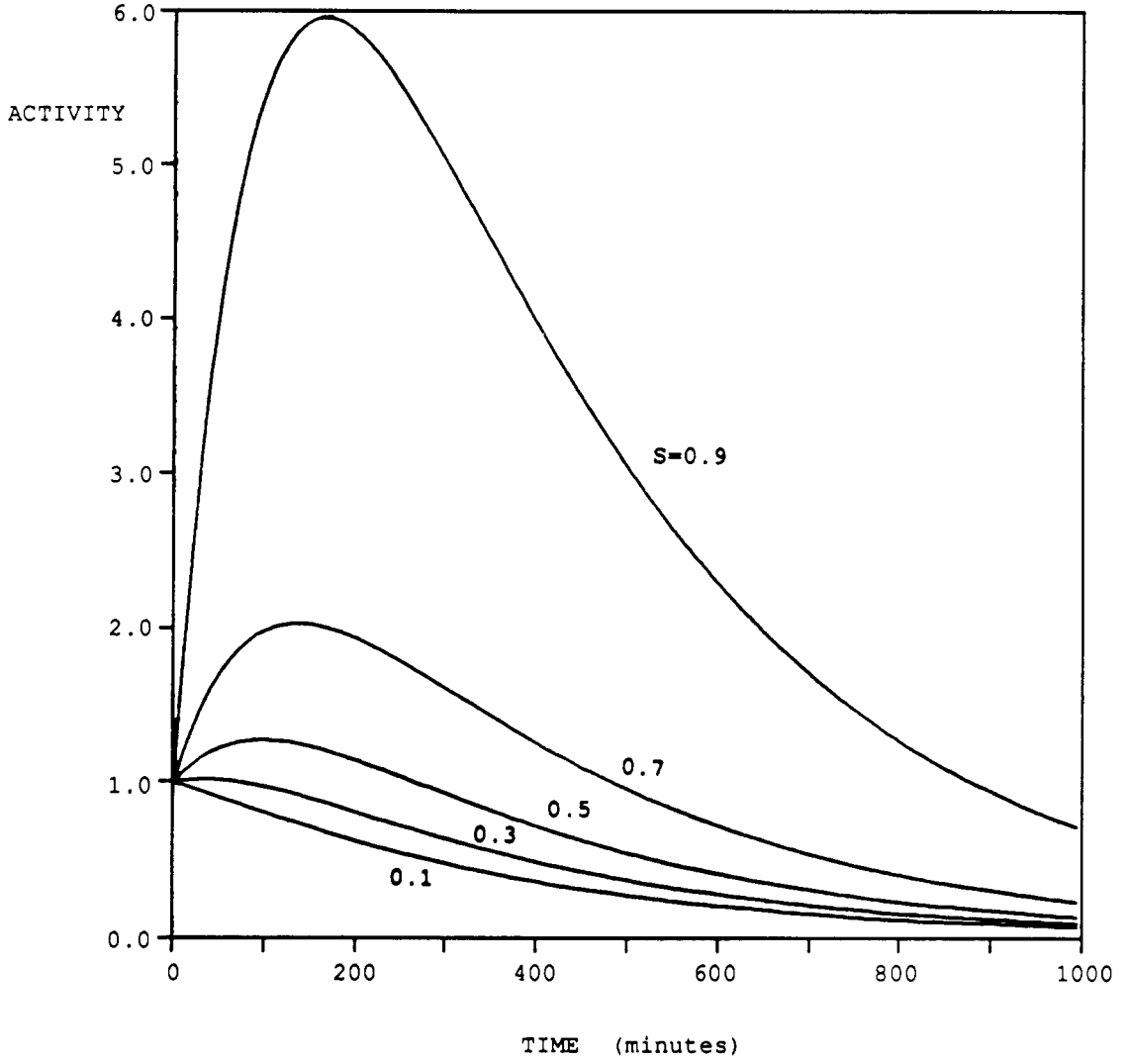

Figure 7. Activity versus time curves for different values of the initial fraction of potentially active sites, S ($\psi_a = 10^{-3}$, $\psi_d = 3 \times 10^{-3}$, $m = 1$).

maximum activity obtained decrease when the deactivation function is increased (faster deactivation), especially when the process is started with a low percentage of AS (high S). As was shown in Figure 5B, the maximum of the activity also appears earlier (lower values of t_{max}), when ψ_d is increased. In this respect, the effects of ψ_a and ψ_d are coincident, although due to different reasons: Increases in ψ_a decrease t_{max} by increasing the rate of activation, while increases in ψ_d decrease t_{max} due to a faster increase of the deactivation rate (the activity maximum is reached when both rates equal each other). Figure 6C shows that an increase in a_{pm} is obtained for higher values of ψ_d, which, as shown in the discussion of the influence of h, is a consequence of the decrease in t_{max}.

Influence of the Initial State of the Catalyst. From the results of the parametric study discussed above, it seems clear that the initial state of the catalyst, S, plays a fundamental role in determining the subsequent evolution of the activity in the process. In fact, as Figure 7 shows, by varying the value of S, the evolution of activity can be altered in such a way that no maximum appears, and a deactivation-only process seems to take place. However, if the initial proportion of PAS is significant (such as in curves with $S = 0.1$ and $S = 0.3$ of Figure 7), the activation process must be taken into account in order to obtain meaningful deactivation kinetics, even if activity maxima are not observed. Thus, for instance, a_{pm} for the case of $S = 0.3$ in Figure 7 was 0.71. This means that over 70% of the initial PAS is to be activated during the period of decreasing activity, which will certainly affect the observed deactivation kinetics.

4. Application of the Model to Experimental Data

Fuentes et al. (1982) studied n-butane isomerization on an aluminum chloride/sulfonic acid resin catalyst, in the presence of HCl, using an isothermal differential reactor. In the analysis of the influence of temperature on catalyst deactivation, these authors found that the rate of butane isomerization reaches a maximum and then decreases (Figure 4 of the reference cited). This behavior can be explained by using an activation–deactivation model. In addition, the deactivation process could be reversible, in which case a residual activity would appear. The experimental data obtained by these authors at four temperatures ranging from 343 to 373 K have been fitted to eqs 19 and 20 (reversible deactivation) and to eqs 21 and 22 (irreversible deactivation), in order to find values for the initial reaction rate $(r_A)_0$, as well as for ψ_a, ψ_d, ψ_s, and S at each temperature, for a given set of values of e, m, and h. In preliminary runs, we did not find statistically significant differences between least-squares fits assuming all kinetic orders equal to one ($e = m = h = 1$) and other possible combinations of values of e, m, and h. Therefore, these

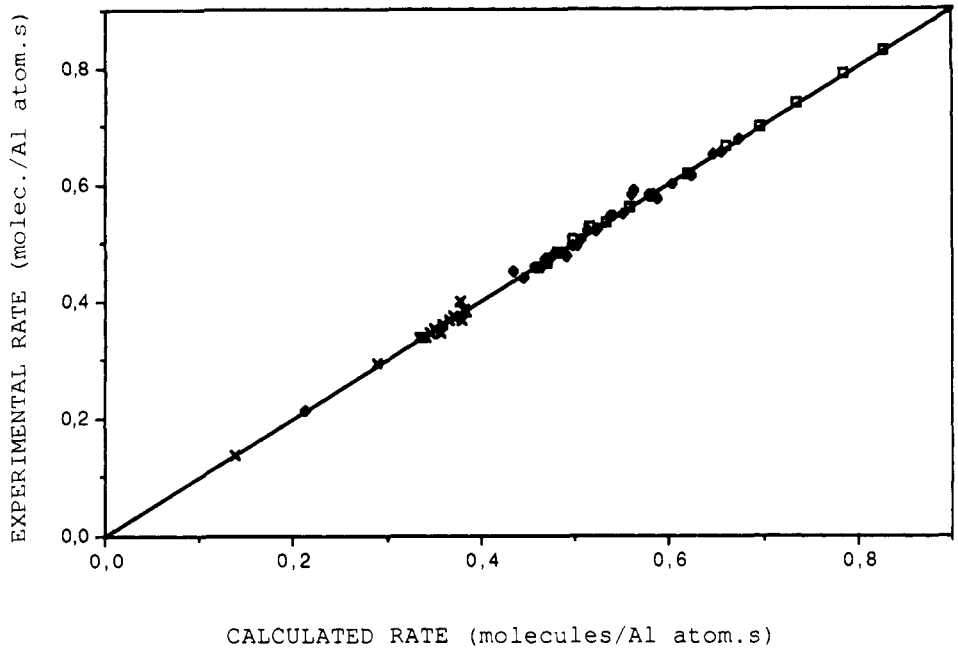

Figure 8. Adequacy of fit of the experimental data (Fuentes et al., 1982), by the model presented in this work. (×) 70 °C; (◇) 80 °C; (◆) 90 °C; (□) 100 °C.

Table III. Comparison of Data Fit with Models A and B[a]

T, K	CR	$F(1, \vartheta_2, 95\%)$	$F(1, \vartheta_2, 99\%)$
343	0.035	4.96 ($\vartheta_2 = 10$)	10.04
353	0.319	4.84 ($\vartheta_2 = 11$)	9.65
363	5.987	4.84 ($\vartheta_2 = 11$)	9.65
373	28.27	4.96 ($\vartheta_2 = 10$)	10.04

[a] $F(\vartheta_1, \vartheta_2, (1-\alpha)\%)$; $\vartheta_1 = n_A - n_B = 1$; $\vartheta_2 = N_p - n_A$.

were taken as one, and the equations to be used for eqs 19–22.

From the definition of activity given above, these equations are transformed as follows:

model A: reversible deactivation

$$(r_A)_t = (r_A)_0\{a_s + B\exp(-\psi_a t) + (1 - a_s - B)\exp[-(\psi_d + \psi_a)t]\} \quad (26)$$

where a_s and B are given by eqs 21a and 21b, respectively

model B: irreversible deactivation

$$(-r_A)t = (-r_A)_0[C\exp(-\psi_a t) + (1 - C)\exp(-\psi_d t)] \quad (27)$$

where C is given by eq 23.

There are five parameters to be obtained in model A, namely, ψ_a, ψ_d, ψ_s, $-r_A$, and S, and four in model B (since $\psi_s = 0$). Both models have therefore been used to fit the experimental data at four different temperatures, and statistical tests have been carried out on the results in order to compare both fits. The comparison between models A and B was done by means of an F-test. To this end, a "comparison coefficient", CR (Lin et al., 1983), was calculated as

$$\mathrm{CR} = \frac{(\sum e_B^2 - \sum e_A^2)/(n_A - n_B)}{\sum e_B^2/(N_p - n_A)} \quad (28)$$

where $\sum e_A^2$ and $\sum e_B^2$ represent the minimum sum of squared deviations for models A and B, respectively. The value of CR was compared with the value of F, calculated as $F(n_A - n_B, N_p - n_A, 1 - \alpha)$, where $1 - \alpha$ is the level of confidence selected. Model A was considered to be significantly better for the cases in which CR > F. The results of the test are shown in Table III where it can be seen that the model of five parameters (model A) gives a significantly better fit at 363 and 373 K, while the model with four parameters fit the data better at 343 and 353 K (lower temperatures).

With the above considerations, a nonlinear least-squares fit of the experimental data has been carried out, which yielded the parameters in Table IV. These were obtained by minimizing the objective function: $\sum((-r_A) - (-\hat{r}_A))^2$. A very satisfactory fit was obtained for the experimental data available, as shown in Figure 8.

In Table IV, the best Arrhenius law fit was obtained for the initial reaction rate (regression coefficient = 0.9995), with a preexponential factor of 9.029×10^3 molecules/(Al atom·s) and an activation energy for the butane isomerization of 10696 cal/mol. Less satisfactory fits were obtained for ψ_a and ψ_d. This was an expected result, since ψ_a, ψ_d, and ψ_s are more complex functions of composition and temperature (eq 16), and therefore, an Arrhenius law is not likely to give a satisfactory fit of their variation with temperature.

Table IV. Variation of the Model Parameters with Temperature[a]

T, K	$10^3((-r_A)_0) \pm$ SE	$\psi_a \pm$ SE	$10^3(\psi_d \pm$ SE)	$10^3(\psi_s \pm$ SE)	$S \pm$ SE
343	1.378 ± 0.009	0.067 ± 0.005	0.85 ± 0.12	0.0	0.66 ± 0.021
353	2.13 ± 0.012	0.19 ± 0.019	1.56 ± 0.098	0.0	0.65 ± 0.019
363	3.36 ± 0.012	0.18 ± 0.015	2.76 ± 0.085	2.9 ± 0.72	0.53 ± 0.013
373	4.81 ± 0.010	0.29 ± 0.039	4.22 ± 0.053	3.2 ± 0.25	0.452 ± 0.007

[a] Units: $(-r_A)_0$, molecules/(Al atom·s); ψ, min^{-1}. SE, standard error.

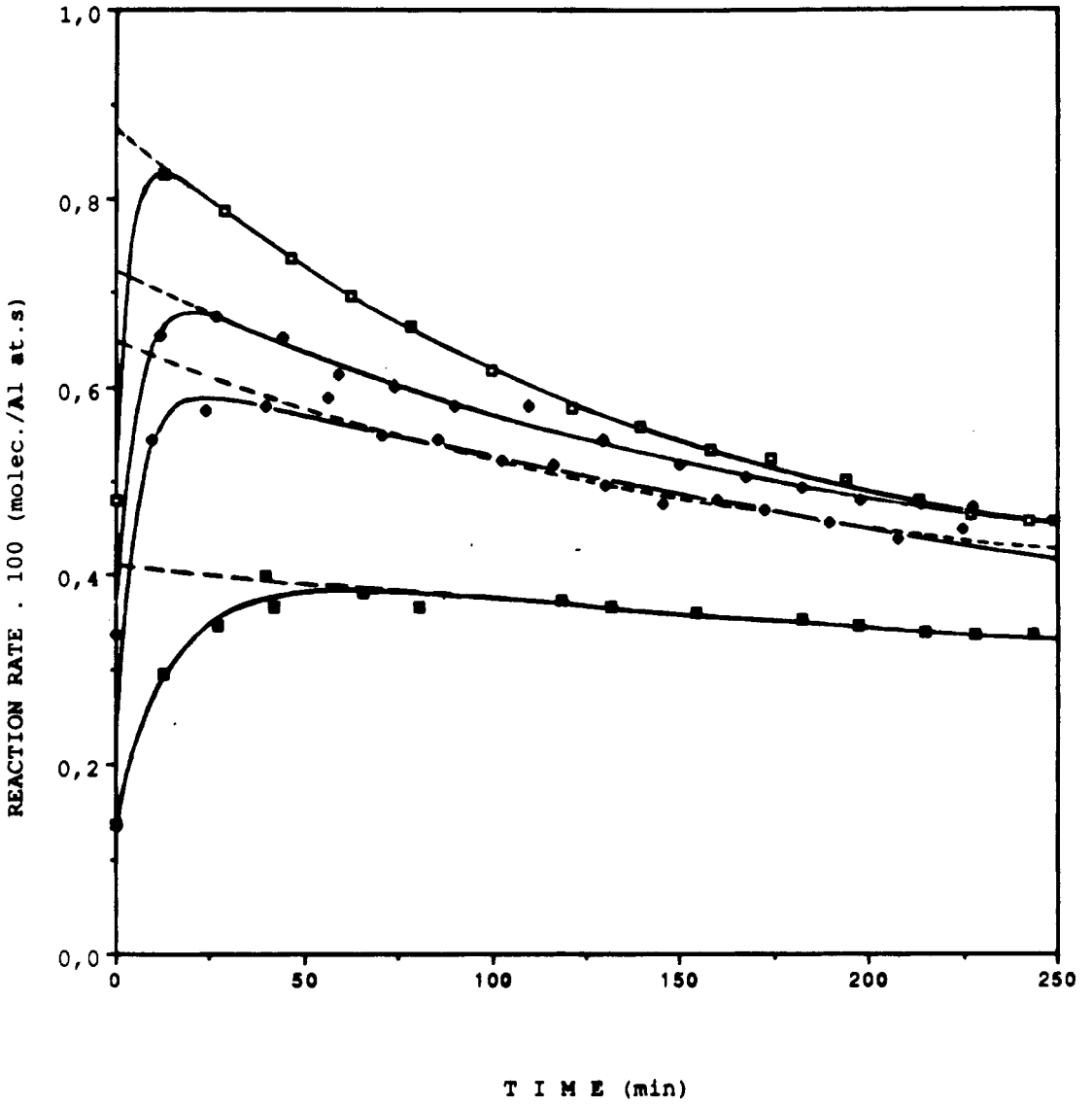

Figure 9. Fit of experimental data of Fuentes et al. (1982) by the reversible deactivation model (discontinuous line) and by the activation–deactivation model (full line).

The initial fractions of potentially active sites, S, given in Table IV are all between 0.45 and 0.66 for the different samples, thus indicating similar activation procedures. In particular, the initial fractions of PAS at the lower temperatures are practically coincident. On the other hand, the model equations allow the calculation of t_{max}, a_{max}, a_s, and a_{pm}, from the values of the parameters in Table IV. The results are shown in Table V.

The variation in the initial potential activity of the catalyst, S (according to the results in Table IV in the experiments at 343 and 373 K, about 66% and 45% of the sites respectively remained to be activated), can be explained by the difficulties in obtaining sample homogeneity during pretreatments, as pointed out by Fuentes et al. (1982). The pretreatment procedure consisted of reacting $AlCl_3$ on a N_2 stream at 140 °C with different catalytic supports. The authors state that the incorporation of aluminum chloride into the packed bed was nonuniform. Also, the Al/S and Cl/Al atomic ratios varied widely. This led to variations in catalytic activity from position to position in the packed bed and also from one preparation to another. Within this context, the variation obtained for S can easily be accommodated.

The increase in catalytic activity observed during the initial stages of the reaction when 22% HCl was added to

Table V. Variation of a_{max}, a_{pm}, a_s, and $(-r_A)_s$ with Temperature

T, K	t_{max}, min	a_{max}	a_{pm}	a_s	r_s, 10^3molecules/(Al atom·s)
343	59.6	2.80	0.018	0	0
353	23.2	2.76	0.012	0	0
363	19.9	2.02	0.025	1.10	3.71
373	12.3	1.72	0.030	0.781	3.26

to the feed seems to be related to the formation of proton–donor groups in the catalyst. Fuentes et al. (1982) also found a correlation between the catalytic activity for n-butane isomerization and the atomic ratio Cl/Al of the catalyst. When HCl was not present in the feed, the resins rapidly lost activity, becoming almost inactive within 1 h on stream (Dooley and Gates, 1985). When the adsorbed HCl was removed by heating overnight under vacuum, the catalyst were rendered inactive. All the above seems to indicate that an interaction of HCl with the catalytic surface is necessary for the activation process.

Catalyst deactivation has been related to the dehalogenation of the catalyst (Dooley and Gates, 1985). This would result in less strongly acidic groups (Fuentes et al., 1982). Catalyst fouling by the polymers formed in the

Table VI. Parameter Values Obtained by Using a Reversible Deactivation Model (Eq 17b)

T, K	N_p	$10^3((-r_A)_0 \pm SE)$	$10^3(\psi_d \pm SE)$	$10^3(\psi_s \pm SE)$	$a_s \pm SE$
343	14	4.13 ± 0.011	0.996 ± 0.050	1.10 ± 1.58	0.52 ± 0.299
353	14	6.48 ± 0.034	2.45 ± 0.15	2.85 ± 1.70	0.54 ± 0.090
363	13	7.23 ± 0.026	2.73 ± 0.086	2.80 ± 0.759	0.51 ± 0.041
373	11	8.74 ± 0.019	4.05 ± 0.050	2.90 ± 0.252	0.42 ± 0.013

[a] Units: $(-r_A)_0$, molecules/(Al atom·s); ψ, min^{-1}. SE, standard error

reaction could also contribute to catalyst deactivation, since traces of higher molecular weight products have been reported (Dooley and Gates, 1985).

Even though the formation and destruction of active sites for this reaction may not be completely elucidated, sufficient evidence has been gathered to suggest that both processes can take place simultaneously, and therefore, an activation–deactivation model is appropriate to deal with the interpretation of kinetic data when HCl is added to the feed.

To have a basis for comparison with conventional deactivation models, the data obtained at the four temperatures at $t > t_{max}$ have been fitted by using a reversible deactivation model (Fuentes, 1985; Corella et al., 1988), which does not take into account the activation stage of the catalyst. A good fit was obtained for the data beyond t_{max}, as can be observed in Figure 9, where the curves obtained from the reversible deactivation model and the model presented in this work are practically coincident after approximately 30 min on stream. However, the kinetic parameters obtained from the two models are rather different, as shown by the comparison of the results presented in Tables IV and V and those in Table VI, where the values calculated for comparable model parameters ($(-r_A)_0$, ψ_d, and a_s) are presented. An Arrhenius fit of the values of the initial rate of the main reaction obtained in this case gave a preexponential factor of 31.1 molecules/(Al atom·s) and an activation energy of 6031 cal/mol, which is about 44% lower than that predicted by the activation–deactivation model.

Taking into account that when the maximum activity is reached the catalyst is almost completely activated (a_{pm} for all temperatures was equal or less than 3%), this case could have been regarded on an a priori basis as a favorable one in terms of expected agreement between the deactivation-only and the activation–deactivation models. The fact that even in this case they differ considerably shows the need for a more general approach that considers activation processes when they take place simultaneously with deactivation, even if only a decrease in activity is observed. This is especially true if the kinetic parameters obtained are to be employed for extrapolation to conditions out of the range studied or when catalyst particles and/or reactors are to be modeled.

5. Conclusions

A kinetic model has been developed to describe the evolution of the activity of a catalyst when activation and deactivation processes take place simultaneously with the main reaction. The study of the influence of the different parameters of the model shows that the initial state of the catalyst, S, is usually the dominant factor in determining the pattern of evolution of the catalytic activity. However, different combinations of values of the model parameters may give rise to very different situations, in which activity maxima can be enhanced, reduced, or even completely eliminated.

The application of the model to experimental data show that the values of the parameters obtained in kinetic studies can change considerably when the activation process is taken into account, even for cases in which there were relatively few PAS remaining when the maximum of activity was reached.

Acknowledgment

This research was funded by DGICYT, Spain, Project PB87-631.

Nomenclature

a = activity of the catalyst, defined by eq 12
A, R, S = reactant and products of the main reaction
a_{max} = maximum activity
a_p = potential activity, defined by eq 11
a_{pm} = potential activity at t_{max}
a_s = residual activity for very long times
B = coefficient defined by eq 21b
C = coefficient defined by eq 23
C^*_{il} = concentration of potentially active sites covered by component i (i = A, R, S, M, N, P), mol/g of catalyst
C^*_l = concentration of vacant potentially active sites, mol/g of catalyst
CR = comparison coefficient (eq 28)
C_{il} = concentration of active sites covered by component i (i = A, R, S, M, N, P), mol/g of catalyst
C_l = concentration of vacant active sites, mol/g of catalyst
$C_{l'}$ = concentration of deactivated sites, mol/g of catalyst
d = order of deactivation, defined by eq 16
d_m = kinetic order, defined by eq 16
e = number of active sites that take part in the controlling step of the activation process
h = number of active sites that take part in the controlling step of the deactivation reaction
K = equilibrium constant of the main reaction, atm^{-1}
k = kinetic constant of the main reaction, s^{-1}
k_a = kinetic constant of the activation reaction, s^{-1}
k_d' = kinetic constant of the reverse deactivation reaction, s^{-1}
k_d = kinetic constant of the direct deactivation reaction, s^{-1}
K^* = equilibrium constant for adsorption on the potentially active sites, atm^{-1}
K_i = equilibrium constant for the adsorption on the active sites (i = A, R, S, M, N), atm^{-1}
L = total concentration of active sites, mol of sites/g
l = active site (AS)
l′ = deactivated site (DS)
L^* = total concentration of potentially active sites, mol of sites/g
l* = potentially active site (PAS)
M = substance (reactant, product, both, impurity, etc.) that reacts with a potentially active site giving some active sites
m = number of active sites that take part in the controlling step of the main reaction
M′ = species produced in the activation reaction
N = species (reactant, product, both, impurity, etc.) that gives rise to the coke precursor
N′ = species produced in the deactivation reaction
n_A = number of parameters of model A (eq 28)
n_B = number of parameters of model B (eq 28)
N_p = number of experimental data points (eq 28)
p_i = partial pressure of component i (i = A, R, S, M, N), atm
P = coke precursor
$-r_A$ = main reaction rate, molecules/(Al atom·s)

$-r_s$ = residual rate (Tables VI and VII), molecules/(Al atom·s)
S = initial state of the catalytic sites, defined by eq 16
T = temperature, °C or K
t = time-on-stream, s
t_{max} = time at which the maximum activity is reached

Greek Symbols

α,β = parameters defined by eq 9
$\psi_a(p_i,T)$ = activation function defined by eq 16
$\psi_d(p_i,T)$ = deactivation function defined by eq 16
$\psi_s(p_i,T)$ = regeneration function (related to reversible deactivation), eq 16
ϑ_1, ϑ_2 = number of degrees of freedom in F-test

Appendix: Statistical Treatment

The method used in the parametric study presented earlier involves the selection of a given number of "levels" (i.e., selected values) for all the parameters studied (Box et al., 1978). Equations 13 and 15 are then solved for all the sets of parameter values considered, and the corresponding activity versus time curves are obtained. This yields the values of a_{max}, t_{max}, and a_{pm} for each of the different combinations of parameter values. Of the seven parameters, two have been studied at three levels and four at two levels, and the value of one (ψ_s) has been kept constant throughout the study. This yields 144 simulations distributed as follows: (a) measurement of the effect of m, e, h, and ψ_a, 72 simulations for each of the two levels studied; (b) measurement of the effect of S and ψ_d, 48 simulations for each of the three levels studied.

The number of levels for each parameter as well as the values employed are given in Table VII. Thus, with relatively few simulations, a wide range of parameter values can be explored, and preliminary analyses can be carried out the individual effects of the different parameters on the system behavior.

The average results obtained in the 144 simulations carried out were as follows: average a_{max}, 4.02; average t_{max}, 137.6 min; and average a_{pm}, 0.200.

These values are used as a reference to quantify the importance of the effects of the different parameters. By "individual effect" of a parameter we denote the change observed in a given system response when the value of the parameter changes from one level to another (e.g., in parameters with two levels, we refer to the change from low level, L, to the high level, H). Thus, the effect obtained when m changes from 1 to 2 can be quantified by the differences $\{a_{max}(m=1) - a_{max}(m=2)\}$; $\{t_{max}(m=1) - t_{max}(m=2)\}$, and $\{a_{pm}(m=1) - a_{pm}(m=2)\}$. These represent the individual effect of m on a_{max}, t_{max}, and a_{pm}, respectively.

In the present study, when each of the remaining parameters are varied, 72 values of a_{max}, t_{max}, and a_{pm} are obtained for each level of m. Thus, 72 individual effects of m can be calculated. The average of these different individual effects referring to a particular response (e.g., a_{max}) is called the *main* effect of m on this response (Box et al., 1978) and measures the average effect of m over all conditions of the other parameters.

This procedure for the calculation of the influence of a parameter has some advantages over the alternative of varying the parameter under study while holding the rest constant at selected values, since this implicitly assumes that the effect observed would be the same for any set of selected values of the other parameters. This assumption clearly does not hold true in the case presented, as was shown in Figures 1 and 2. For the case studied, the results of the 144 simulations carried out showed that, on average, when m was varied from 1 to 2, a_{max} increased 3.979 units, t_{max} increased 42.19 min, and a_{pm} decreased 0.0668 units,

Table VII. Parameter Values Used in the Simulations

	level				level		
	high	med	low		high	med	low
m	2		1	ψ_a	0.1		0.01
e	2		1	ψ_d	0.003	0.001	0.0003
h	2		1	S	0.8	0.5	0.2

i.e., the main effects of m on a_{max}, t_{max}, and a_{pm} were −3.979, −42.19 min, and 0.0668, respectively.

The *interaction between two parameters* (e.g., m and S) is given by one-half of the difference between the average effect of m at two different levels (L and H) of S (Box et al., 1978). We denote this interaction by mS and express it by

$$mS = \frac{1}{2}[a^m_{max}\}_{S=0.8} - a^m_{max}\}_{S=0.2}] = -2.252$$

where $a^m_{max}\}_{S=0.2}$ and $a^m_{max}\}_{S=0.8}$ represent the average effect of m on a_{max} at S = 0.2 and 0.8, respectively.

Registry No. $CH_3(CH_2)_2CH_3$, 106-97-8; $AlCl_3$, 7446-70-0.

Literature Cited

Agorreta, E.; Santamaria, J.; Menéndez, M.; Monzón, A. Modelado cinético de sistemas catalíticos sometidos a fenómenos de activación/desactivación. *Proc. 11th Iberoam. Symp. Catal., Guanajuato* **1988**, *1*, 885.

Agorreta, E.; Santamaria, J.; Coronas, J.; Monzón, A. Manuscript in preparation, 1990.

Amariglio, A.; Amariglio, H. Unexpected and progressive self-reaction of rhodium catalyzing the H_2–O_2 reaction after an immediate inhibition by C_2H_4 added to the reactant mixture: parallel activation in C_2H_4 hydrogenation. *J. Catal.* **1981**, *68*, 487–491.

Amariglio, A.; Lakhdar, M.; Amariglio, H. Catalytic activation of Rhodium, revealed by C_2H_4 hydrogenation and resulting from preincorporation of O_2 and back-diffusion to its surface under H_2 exposure. *Proc. 7th Int. Congress Catal., Tokyo* **1980**, 669–681.

Amariglio, A.; Lakhdar, M.; Amariglio, H. Methanation of carbon dioxide over preoxidized Rhodium. *J. Catal.* **1983**, *81*, 247–251.

Box, G. E. P.; Hunter, W. G.; Hunter, J. S. *Statistics for experimenters*; J. Wiley and Sons: New York, 1978.

Brito, J.; Golding, R.; Severino, F.; Laine, J. Relations between coke deposition and activity of HDS catalysts. *Prepr. Pap.—Am. Chem. Soc., Div. Pet. Chem.* **1982**, *27*, 762–771.

Bukur, D. B.; Mukesh, D.; Patel, S. A. Promoter effects on precipitated iron catalyst for Fischer–Tropsch Synthesis. *Ind. Eng. Chem. Res.* **1989**, *29*, 194–204.

Corella, J.; Asúa, J. M. Kinetic equations of mechanistic type with nonseparable variables for catalyst deactivation by coke. Models and data analysis methods. *Ind. Eng. Chem. Process Des. Dev.* **1982**, *21*, 55–61.

Corella, J.; Adánez J.; Monzón, A. Some intrinsic kinetic equations and deactivation mechanisms leading to deactivation curves with a residual activity. *Ind. Eng. Chem. Res.* **1988**, *27*, 375.

Cunningham, J.; Al-Sayyed, G. H.; Cronin, J. A.; Fierro, J. L. G.; Healy, C.; Hirchwald, W.; Ilyas, M.; Tobin, J. P. Surface synergisms between copper and its oxides. *J. Catal.* **1986**, *102*, 160–171.

Dooley, K. M.; Gates, B. C. Paraffin isomerization by polymer supported superacids. *J. Catal.* **1985**, *96*, 347–356.

Dry, M. E. The Fisher-Tropsch synthesis. In *Catalysis Science and Technology 1*; Anderson, J. R., Boudart, M., Eds.; Springer-Verlag: New York, 1981; pp 159–255.

Fuentes, G. A. Catalyst deactivation and steady-state activity: a generalized power-law equation model. *Appl. Catal.* **1985**, *15*, 33–40.

Fuentes, G. A.; Boegel, J. V.; Gates, B. C. n-Butane isomerization catalyzed by supported aluminum chloride. *J. Catal.* **1982**, *78*, 436–444.

Hicks, R. F.; Bell, A. T. Effects of metal–support interactions on the hydrogenation of CO over Pd/SiO_2 and Pd/La_2O_3. *J. Catal.* **1984**, *90*, 205–220.

Inioui, A.; Eddouasse, M.; Amariglio, A.; Ehrhardt, J. J.; Alnot, M.; Lambert, J. Catalytic activation of cobalt induced by oxidizing treatments in the methanation of carbon dioxide. *J. Catal.* **1987**, *106*, 144–165.

Kikuchi, E.; Wada, H.; Fujishiro, K.; Chiba, T.; Morita, Y. Synthesis of hydrocarbons from carbon monoxide and steam on precipitat-

ed-iron catalysts. *Int. Chem. Eng.* **1984**, *24* (4), 710-717.
Krebs, H. J.; Bonzel, H. P.; Schwarting, W. Microreactor and electron spectroscopy studies of Fischer-Tropsch synthesis of magnetite. *J. Catal.* **1981**, *72*, 199-209.
Kuivila, C. S.; Stair, P. C.; Butt, J. B. Compositional aspects of Iron Fischer-Tropsch catalysts: an XPS/Reaction study. *J. Catal.* **1989**, *118*, 175-191.
Laine, J.; Brito, J.; Gallardo, J.; Severino, F. The role of nickel in the initial transformations of hydrodesulfurization catalysts. *J. Catal.* **1985**, *91*, 64-68.
Leary, K. J.; Michaelis, J. N.; Stacy, A. M. Carbon and oxygen atom mobility during activation of Mo_2C catalysts. *J. Catal.* **1986**, *101*, 301-313.
Lin, C.; Park, S. W.; Hatcher, W. J. Zeolite catalyst deactivation by coking. *Ind. Eng. Chem. Process Des. Dev.* **1983**, *22*, 609-614.
McDaniel, M. P.; Johnson, M. M. A comparison of Cr/SiO_2 and $Cr/AlPO_4$ polymerization catalysts. *J. Catal.* **1986**, *101*, 446-457.
Montes, M.; Penneman de Bosscheyde, Ch.; Hodnett, B. K.; Delaunay, F.; Grange, P.; Delmon, B. Influence of metal-support interactions on the dispersion, distribution, reductibility and catalytic activity of Ni/SiO_2 catalysts. *Appl. Catal.* **1984**, *12*, 309-330.
Nix, R. M.; Judd, R. W.; Lambert, R. M.; Jennings, J. R.; Owen, G. High-activity methanol synthesis catalysts derived from rare-earth/Copper precursors: Genesis and deactivation of the catalytic system. *J. Catal.* **1989**, *118*, 175-191.
Noelke, C. J.; Rase, H. F. Improved hydrodechlorination catalysis: chloroform over Platinum-Alumina with special treatments. *Ind. Eng. Chem. Prod. Res. Dev.* **1979**, *18*, 325-328.
Olazar, M.; Aguayo, A. T.; Arandes, J. M.; Azkoiti, M. J.; Bilbao, J. Mecanismos de desactivación de un catalizador de sílice alumina en la polimerización de alcohol bencílico gas. *Proc. 11th Iberoam. Symp. Catal., Guanajuato* **1988**, *1*, 897.
Olazar, M.; Aguayo, A. T.; Arandes, J. M.; Bilbao, J. Polymerization of gaseous benzyl alcohol. 3. Deactivation mechanisms of a SiO_2/Al_2O_3 catalyst. *Ind. Eng. Chem. Res.* **1989**, *28*, 1752.
Perti, D.; Kabel, R. L. Kinetics of CO oxidation over Co_3O_4/γ-Al_2O_3. *AIChE J.* **1985**, *31*, 1420-1426.
Pijolat, M.; Perrichon, V.; Bussiere, P. Study of the carbonization of an iron catalyst during the Fischer-Tropsch synthesis: Influence on its catalytic activity. *J. Catal.* **1987**, *107*, 82-91.
Prada Silvy, R.; Deprez, P.; Berge, P. C.; Martin, M. A.; Grange, P.; Delmon, B. Activación de catalizadores de hidrodesulfuración: Influencia del coque en la etapa inicial de reducción-sulfuración sobre las propiedades fisico-químicas y catalíticas. *Proc. 11th Iberoam. Symp. Catal., Guanajuato* **1988**, *2*, 1051.
Szépe, S.; Levenspiel, O. Catalyst deactivation. *Proceedings of the 4th European Symposium on Chemical Reaction Engineering. Brussels, September 1968*; Pergamon Press: Oxford, 1971.
Tau, L. M.; Bennet, C. O. The oxidation effect on the CO/H_2 reaction over Titania-supported Fe catalysts. *J. Catal.* **1985**, *96*, 408-419.

Received for review April 6, 1990
Revised manuscript received July 30, 1990
Accepted August 10, 1990

Camet Oxidation Catalyst for Cogeneration Applications

Franklin J. Gulian, Jeffery S. Rieck, and Carmo J. Pereira*
W. R. Grace & Company, Research Division, 7379 Route 32, Columbia, Maryland 21044

Environmental pollution control regulations have required the use of oxidation catalysts to reduce emissions of carbon monoxide and unburned hydrocarbons from cogeneration plants. Oxidation catalyst performance requirements include low pressure drop and high conversion efficiency. The conversion limit is controlled by external mass-transfer limitations determined by the properties of the monolith substrate. Conventional monoliths contain identical channels that pass straight through the monolith and are parallel to the flow direction. This paper discusses the conversion and pressure drop performance of a new metal monolith substrate based on a folded metal foil that is corrugated in a herringbone pattern. The external mass-transfer pressure drop performance of this type of metal monolith catalyst is compared with conventional ceramic substrate based catalysts.

Introduction

During the past few years, standards that limit the emissions of carbon monoxide, hydrocarbons, and nitrogen oxides from stationary sources have been established in the U.S. and in several other nations. Facilities governed by these standards include those operated by independent power producers ranging in size from 1 MW to hundreds of megawatts. Cogeneration is often the preferred power generation option as it offers a high rate of return on investment. These plants typically consist of a natural gas or oil-fired turbine for generating electricity and a Heat Recovery Steam Generation (HRSG) system. The steam generated in the HRSG can be used as process steam or to drive a steam turbine.

Cogeneration plants that are out of compliance on carbon monoxide emissions usually require an oxidation catalyst that removes at least 90% of the carbon monoxide. A low pressure drop through the catalyst (4 in. of water or less) is a necessity since every 4 in. of water backpressure causes a 0.4-1.5 per cent loss of turbine power output (Jung and Becker, 1987). Oxidation catalyst systems are therefore placed as "curtain walls" just before the HRSG system. An example of a curtain wall reactor is shown in Figure 1. Typical reactor dimensions in such a case are 40 ft × 35 ft × 3.5 in. The catalytic reactor contains a number of 2 ft × 2 ft × 3.5 in. catalyst modules.

Carbon monoxide and hydrocarbon emissions are most easily reduced by passing the turbine effluent over a noble metal containing oxidation catalyst. Noble metal oxidation catalyst technology was originally developed nearly 20 years ago for automotive exhaust emission control. Jung and Becker (1987) and Cordonna et al. (1989) have discussed the catalytic chemistry required for the oxidation of carbon monoxide and hydrocarbons in cogeneration effluents. The oxidation conversion limit is controlled by external mass-transfer limitations that are determined by the properties of the monolithic substrate. Thus, there is considerable incentive for developing substrates having improved external mass-transfer characteristics.

Ceramic or metal monolith-supported noble metal catalyst systems can be designed to provide the high conversion efficiency and low pressure drop required in cogeneration applications. Conventional monoliths contain identical channels that pass straight through the monolith and are parallel to the flow direction. The mass-transfer and pressure drop characteristics of such monoliths have been quantified by Hegedus (1973).

* Author to whom correspondence is to be addressed.

0888-5885/91/2630-0122$02.50/0